Geochimica et Cosmochimica Acta 356 (2023) 116–128

Contents lists available at ScienceDirect

Geochimica et Cosmochimica Acta

journal homepage: www.elsevier.com/locate/gca

Equilibrium partitioning and isotopic fractionation of nitrogen between biotite, plagioclase, and K-feldspar during magmatic differentiation

Toby J. Boocock [a], Eva E. Stüeken [a], Grant M. Bybee [b], Ramona König [a], Adrian J. Boyce [c], Julie Prytulak [d], Iris Buisman [e], Sami Mikhail [a,*]

[a] School of Earth and Environmental Sciences, University of St Andrews, UK
[b] School of Geosciences, University of the Witwatersrand, South Africa
[c] Scottish Universities Environmental Research Centre, UK
[d] Department of Earth Sciences, Durham University, UK
[e] Department of Earth Sciences, University of Cambridge, UK

ARTICLE INFO

Associate editor: Ralf Halama

Keywords:
Magmatic differentiation
Elemental partitioning
Stable isotope fractionation
Nitrogen geochemistry

ABSTRACT

A significant portion of the continental crust is composed of plutonic igneous rocks. However, little is known about the geochemical behaviour of N between the different minerals during magmatic differentiation. To provide new constraints for the behaviour of N during crust formation, we have characterised the geochemistry of nitrogen (N) in the compositionally zoned calc-alkaline pluton at Loch Doon, SW Scotland. We present N concentration and N isotope values for whole-rock data alongside biotite, plagioclase and K-feldspar mineral separates and assess the degree to which these data preserve equilibrium partitioning during magmatic differentiation. We show that whole rock likely inherited its N contents and $\delta^{15}N$ signatures from the initial source composition and that this signature is homogenous at a pluton scale. Whilst the whole-rock data are best explained as crust-derived N in the source, the degree of homogenisation across a pluton scale is inconsistent with empirical N diffusivities, ruling out syn-emplacement crustal assimilation as the source of N. Instead, our data suggest a crustal signature inherited from depth associated with the Iapetus subduction zone. At a mineral scale, we find that N preferentially partitions into the feldspars over mica in this system in the order K-feldspar > plagioclase ≈ biotite > quartz, with average mineral–mineral distribution coefficients of $D_{N\ plagioclase\text{-}biotite} = 1.3 \pm 0.6$ and $D_{N\ Kspar\text{-}biotite} = 2.8 \pm 0.6$. Partitioning is accompanied by a large and near constant equilibrium isotope fractionation factor between biotite and both feldspars (averages are $\Delta^{15}N_{Plag\text{-}Biotite} = +7.8 \pm 1.2‰$ and $\Delta^{15}N_{Kspar\text{-}Biotite} = +7.9 \pm 1.0‰$). In contrast, $\Delta^{15}N_{Kspar\text{-}Plagioclase}$ closely approximates 0‰, where both minerals show $\delta^{15}N$ values overlapping with the bulk rock $\delta^{15}N$ values. These results show that mica crystallisation generates a ^{15}N-depleted reservoir within plutonic rocks. Moreover, our dataset suggests that feldspars might be a more significant host of N in the igneous portion of Earth's continental and oceanic crust than previously thought.

1. Introduction

Earth's silicate interior contains more N than the atmosphere, biosphere and oceans combined (Busigny and Bebout, 2013; Marty, 2012). This observation has two major implications for the long-term habitability of our planet. First, it implies that an increase in the release flux of rock-bound N would raise pN_2 in the atmosphere, which can enhance the warming effect of existing greenhouse gases by broadening their absorption lines (Goldblatt et al., 2009; Zerkle et al., 2017). Second, N sourced by weathering of Earth's continental crust is a significant nutrient source to the biosphere, which is especially relevant for organisms that cannot access (fix) atmospheric N_2 gas (Houlton et al., 2018). Therefore, accurate models of climate and nutrient supply on the early Earth and possibly other terrestrial planets require constraints on the reservoirs of rock-bound N (including host minerals) and the exchange flux between Earth's surface and interior. However, little is known about the behaviour of N during crust formation. Previous studies have shown that N in geological materials is lost during

* Corresponding author.
E-mail address: sm342@st-andrews.ac.uk (S. Mikhail).

https://doi.org/10.1016/j.gca.2023.07.010
Received 1 May 2023; Accepted 11 July 2023
Available online 17 July 2023

metamorphism (Bebout and Fogel, 1992; Haendel et al., 1986; Halama et al., 2021) but enriched by hydrothermal alteration (Li et al., 2007; Li and Li, 2023a; 2023b; Stüeken et al., 2021). Furthermore, data support conflicting notions that N is either almost totally lost (Elkins et al., 2006; Fischer et al., 2002; Halama et al., 2021) or fully retained (Barry and Hilton, 2016; Busigny et al., 2003) during subduction, depending on P-T conditions of the system studied (Kupriyanov et al., 2022; Harris et al., 2022). Nitrogen stable isotope data from volcanic (Hilton et al., 2002; Sano et al., 2001; Barry and Hilton, 2016; Boocock et al., 2023) and mantle (Halama et al., 2014; Labidi et al., 2020; Marty and Dauphas, 2003) samples confirm that Earth's interior contains a significant isotopic component which overlaps with Earth's surficial (mostly biogenic) N reservoir (Stüeken et al., 2016). In summary, the spread of $\delta^{15}N$ values for mantle samples show a range of 80‰ with an average at -5 ± 3‰, whereas Earth's surficial (mostly biogenic) N reservoir typically averages positive $\delta^{15}N$ values (average $= +5 \pm 4$‰), indicating that surficial N may be transferred to and stored at depth (see Cartigny et al., 2014 for a review). However, it remains poorly constrained how N behaves during the crystallisation of silicate melts. Whilst a number of studies have examined the behaviour of N in igneous systems, there still remain key gaps in igneous N research. In particular, almost all N data for plutonic igneous rocks are whole rock measurements (Ahadnejad et al., 2011; Bebout et al., 1999; Boyd, 1997; Boyd et al., 1993; Cooper and Bradley, 1990; Hall, 1999, 1988, 1987; Hall et al., 1996; Itihara and Honma, 1979; Mao et al., 2003; Zhang, 1988) from which no information can be extracted about mineral–mineral or mineral-melt partitioning. Ergo, all current geochemical models of the N cycle suffer from a lack of fundamental data for the partitioning behaviour and stable isotope fractionation of N in igneous systems. Recent research has found that N can behave like lithophile trace elements during igneous differentiation (Boocock et al., 2023), which implies that igneous differentiation should result in a heterogenous distribution of N between igneous minerals, as is the case for large ion lithophile elements (LILE). Therefore, to accurately model the retention of N during crustal differentiation and to quantify the weatherability of rock-bound N at Earth's surface, quantitative data for the distribution (and exchange) coefficients for N between mineral phases are required. The primary aim of this study is to generate these much-needed data. To do so, we have investigated elemental partitioning and stable isotope fractionation of N between biotite, plagioclase, and K-feldspar (Kspar) relative to each other and to the system (whole rock) during magmatic differentiation using the Loch Doon zoned pluton as a case study.

2. Geological context

The Loch Doon pluton is a compositionally zoned calc-alkaline pluton located in the Southern Uplands Terrane in SW Scotland, UK (Fig. 1). The Loch Doon pluton hosts a suite of units typical of calc-alkaline plutons, from dioritic to granitic (Fig. 1). The pluton was emplaced 408 ± 2 million years ago (Halliday et al., 1978) and outcrops at the surface over an area of 130 km^2 (Hines et al., 2018). The magmas were emplaced through a 15 km-thick sequence of imbricated Ordovician greywacke-shale underlain by subducted oceanic crust (Bamford et al., 1978), interpreted as the accretionary prism of the Iapetus suture zone (Leggett et al., 1979; McKerrow et al., 1977). Magma generation for all Southern Uplands Terrane plutons is associated with a breakoff of the underlying subducted Iapetus slab at approximately 430–410 Ma (Miles et al., 2016), followed by nested emplacement of intermediate to evolved plutons within the Southern Uplands Terrane for the following 50–60 Myr, including Loch Doon (Hines et al., 2018). All previous geochemical and petrological evidence supports closed-system fractional crystallisation as the dominant control on the major and trace element systematics at Loch Doon (Gardiner and Reynolds, 1932; Brown et al., 1979; Tindle and Pearce, 1981; Hall, 1987; Hines et al., 2018; Figs. 2–4). Continuous variation in major and trace elements follow expected trends for fractional crystallisation consistent with a decrease

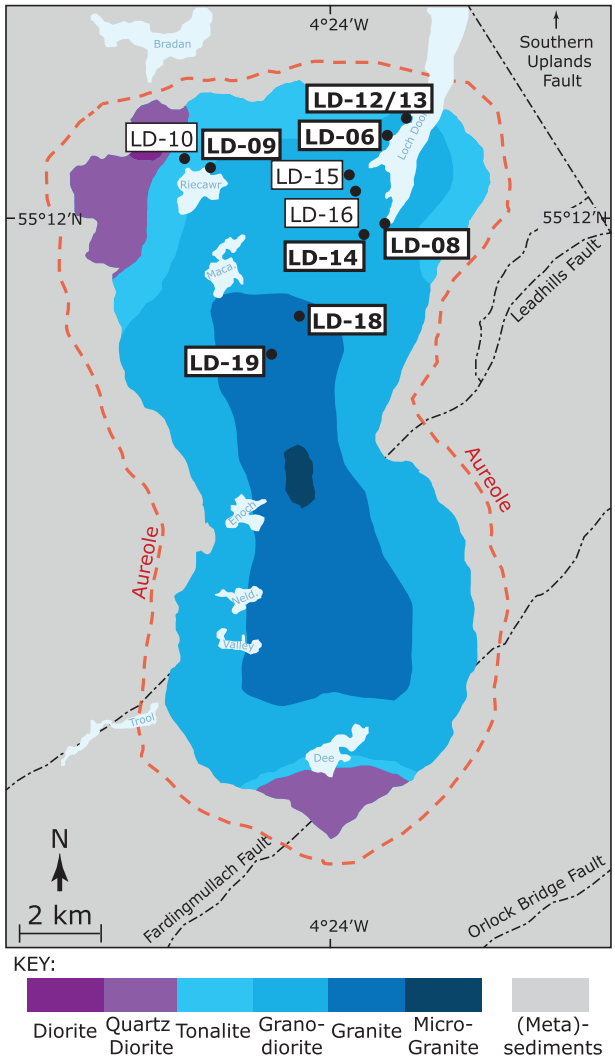

Fig. 1. Geological map of Loch Doon pluton modified after Hines et al. (2018). Sampling locations are shown across the northern limb. Samples in bold represent samples for which mineral separates were picked. * Note sample LD04 is a sample of the local country rock cover taken as a possible N source for the pluton.

in modal abundances of mafic minerals (e.g., pyroxene, actinolite, biotite) and increases in felsic minerals (e.g., Kspar) with progressive differentiation of the magma (Hines et al., 2018; Fig. 4). Isotopic differences between the diorite-granodiorite lithologies and the granites have been interpreted as two generations of melts (Hines et al., 2018; Tindle and Pearce, 1981). The diorite-granodiorite continuum is characterised by an enriched mantle signature of Sr_i near 0.704, εNd of 0, and $\delta^{18}O$ of ca. 6–7‰ (Hines et al., 2018). The more evolved granites in the interior of the pluton project towards Sr_i near 0·712, εNd of −6, and $\delta^{18}O$ of ca. 12‰ and likely indicate a greater degree of crustal assimilation either during melt generation or during magma ascent and emplacement (Hines et al., 2018). However, the continuous and systematic variation in major and trace element trends across both the diorites-granodiorites and the granites, decoupled from the differences in isotopic trends, suggests a genetic linkage between the intermediate and evolved units, where it is possible that some crustal assimilation occurred at depth and is not reflective of high-level crustal assimilation after pluton emplacement. Between all compositional units (e.g., diorite, granodiorite, granite) there are gradational contacts over 10 s-100 s of meters, and both geochemical and lithological variation follow a normal zonation pattern consistent with progressive fractional crystallisation

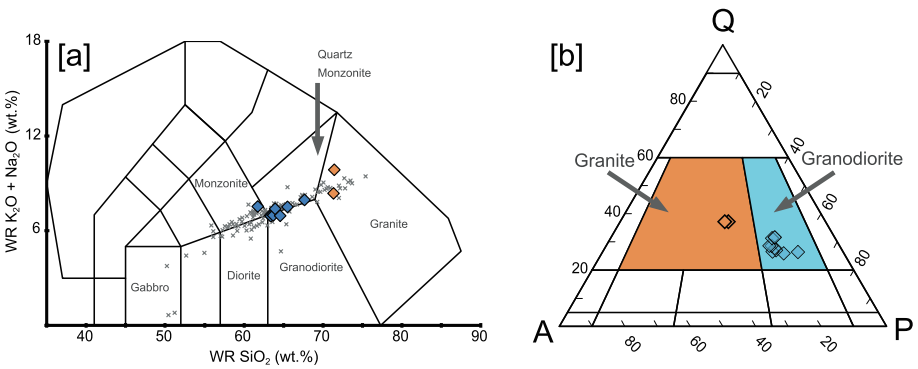

Fig. 2. [a] Plutonic Total Alkali Silica (TAS) diagram (Middlemost, 1994) for the samples from this study (blue and orange diamonds) and compiled literature data (grey crosses) (Brown et al., 1979; Halliday et al., 1980; Tindle and Pearce, 1981; Halliday and Stephens, 1984; Hines et al., 2018). [b] Quartz-Alkali Feldspar–-Plagioclase (QAP) diagram using point counting data from Table 1.

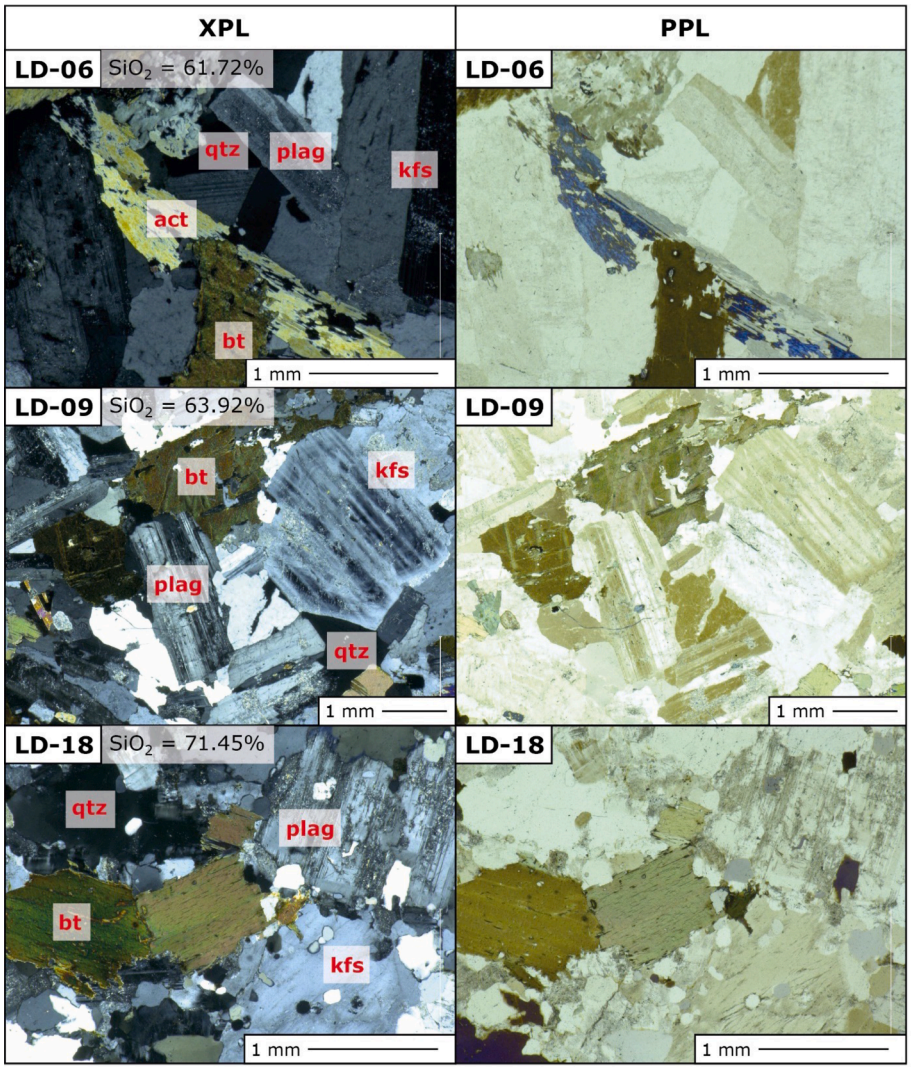

Fig. 3. Thin section images for samples representing the range of lithologies measured in this study. Abbreviations: bt = biotite, qtz = quartz, plag = plagioclase, kfs = Kspar, act = actinolite. Note all biotite, plagioclase and Kspar are generally euhedral indicating across this sample suite these are primary magmatic minerals and not derived via secondary alteration.

geographically from the outer to inner compositions. For the purposes of this study, the relationship – or lack thereof – between the intermediate and evolved units is moot.

2.1. *Sample selection*

We analysed eleven whole-rock samples from the northern section of the Loch Doon pluton. A sub-set of eight samples representing a spread

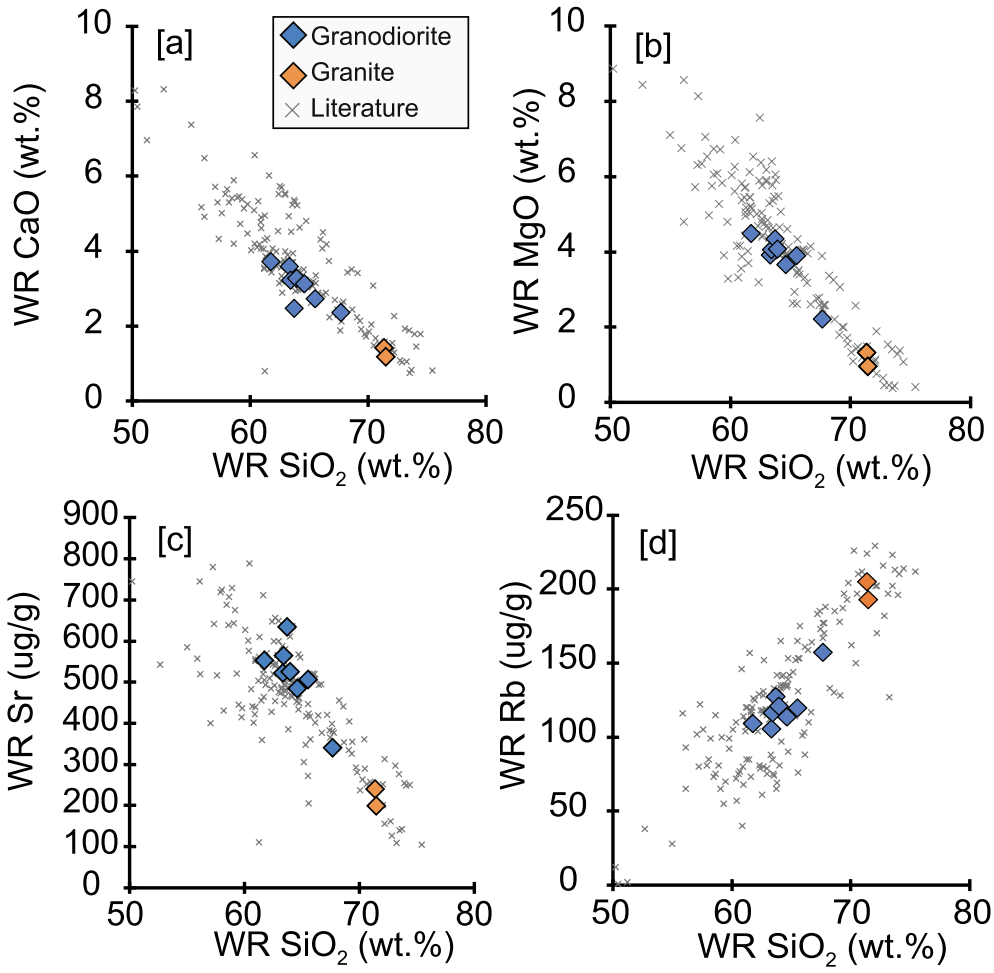

Fig. 4. Major and trace element Harker diagrams for the samples of this study (coloured diamonds) and literature geochemical data (grey crosses) representative of fractional crystallisation.

of rock types were further picked apart. Major and trace element (including N) data were acquired for biotite, plagioclase, and Kspar mineral separates for these samples. Quartz was analysed for N in three samples. The focus was placed on micas and feldspars as they are the most prevalent and likely major N-host phases in igneous systems where fO_2 is >FMQ (Busigny and Bebout, 2013). The eleven whole-rock samples span a narrow range in SiO_2 from diorite to granite, based on TAS classification (Fig. 2a). All samples are phaneritic (>1mm) and comprised dominantly of varying proportions of quartz, plagioclase, Kspar, and biotite (Table 1, Fig. 3). Rock types are assigned using the QAP classification system (Fig. 2b).

For the granodiorite samples, the dominant mineral phases are plagioclase (36–42%), quartz (19–26%), Kspar (15–21%) and biotite (12–15%), with some samples containing up to 5–9% actinolite. The actinolite is interpreted as sub-solidus alteration of primary pyroxenes that are commonly found in the more mafic (i.e., dioritic) compositions, which were not sampled in this study (Brown et al., 1979). There is a shift away from crystallising pyroxenes and amphiboles as the system evolves and biotite becomes the dominant ferromagnesian phase (12–15%) in the granodiorite compositions. Accessory mineral phases in the granodiorites include apatite, sphene, allanite and zircon. In our granitic samples, the modal abundance of the phases is quartz (35%), Kspar (28–29%), plagioclase (30–31%) and biotite (5–6%). Accessory minerals phases include cordierite, apatite, muscovite, zircon, and monazite. One sample of the surrounding greywacke from beyond the pluton aureole was collected to assess local sedimentary N contents as a possible source of N to the pluton (discussed in Section 5.2).

Table 1
Sample modal mineral composition determined by point counting for each lithological unit in this study (with 1 thin section per sample). Remaining mineral % are largely representing actinolite and minor amounts of pyroxene in the granodioritic compositions.

Sample ID	Picked	QAP Classification	Qtz	Kspar	Plag	Biotite	Total
LD-19-06	*Y*	*Granodiorite*	19	10	43	19	91
LD-19-12	*Y*	*Granodiorite*	21	15	45	12	93
LD-19-13	*Y*	*Granodiorite*	20	15	39	14	88
LD-19-14	*Y*	*Granodiorite*	21	17	41	11	90
LD-19-15	*N*	*Granodiorite*	22	16	41	13	92
LD-19-09	*Y*	*Granodiorite*	22	16	39	19	96
LD-19-16	*N*	*Granodiorite*	24	18	42	8	92
LD-19-08	*Y*	*Granodiorite*	26	16	41	13	96
LD-19-10	*N*	*Granodiorite*	26	15	41	15	97
LD-19-19	*Y*	*Granite*	35	28	31	6	100
LD-19-18	*Y*	*Granite*	35	29	30	5	99

3. Methods

3.1. Sample preparation

Samples (generally >1–2 kg) were prepared at the University of St Andrews using the following protocols. Weathered surfaces were removed using a water-cooled rock saw. Small chips of representative and visibly unweathered material, roughly 1 cm^2 in cross section, were mounted in epoxy resin and polished for mineral-specific *in situ* EPMA and LA-ICPMS major and trace element analyses. Thin sections for a representative subset were prepared from visibly unweathered sample blocks for optical microscopy. Of the remaining visibly unweathered material, half was powdered and homogenised for whole-rock analyses in a tungsten carbide mill to achieve a particle size <64 μm. The remaining half of the material was partially crushed with a jaw crusher and rock hammer. The crushed material was sieved for the 350–500 μm size fraction from which individual minerals were subsequently picked. To further aid mineral picking, the sieved fraction was passed through a Frantz magnetic separator at a current of 0.4 A to separate the magnetic fraction (generally the mafic minerals). For each of the eight samples chosen for mineral separate work, around 1.0 g of biotite was picked with tweezers under a binocular microscope from the magnetic fraction, and 1.0–1.5 g of plagioclase and Kspar (and quartz in three cases) was picked from the non-magnetic fraction. Pure mineral separates (>97% purity based on optical inspection) were powdered by hand in an agate pestle and mortar which was cleaned between samples with DI water and reagent-grade ethanol and thoroughly dried.

To ensure cleanliness of the powdered mineral separates for N geochemical analysis, each powder was weighed into pre-combusted (500 °C overnight) glass centrifuge tubes and sequentially washed three times with de-ionised water (18.2 $M\Omega \bullet cm^{-1}$) and ethanol. This brief time interval was sufficient for removing potential contaminants such as fingerprint residue and organic dust (as evidenced by low N contents in quartz; see below), which can be a concern when measuring trace quantities nitrogen. After each step the tubes were centrifuged for 10 min, and the solutions were decanted with no observable loss of powder. The cleaned residue was placed in a drying oven at 70 °C for 48 hrs. Note that the whole-rock powders used for XRF measurements did not go through this cleaning protocol because it is not required for the quantification of lithophile major and trace elements.

3.2. Nitrogen geochemistry

Nitrogen contents and isotope values were measured on whole-rock and mineral-separate powders (biotite, Kspar, plagioclase, quartz) on a MAT253 Isotope Ratio Mass Spectrometer (IRMS) at the University of St Andrews Isotope Geochemistry (STAiG) laboratory, following internally developed and internationally verified protocols (Boocock et al., 2020; 2023). Sample powders were weighed into quartz glass tubes together with ca. 1 g of CuO wire and evacuated overnight at 120 °C to remove air and adsorbed gases. Powders were agitated gently whilst attached to the vacuum line to enhance the removal of any air trapped in the powder pore spaces. After evacuation, the tubes were sealed with an oxy-propane blowtorch and placed into a muffle furnace at 1050 °C for 4 h, followed by 2 h at 600 °C to ensure total liberation of silicate-bound N and conversion to N_2. Note that where we use the term silicate bound N, this N may take the form of differing species such as N_2, NH_4^+, NH_2^-, N^{3-} and as such this method *sensu stricto* measures total silicate N as a bulk analysis. The quartz glass tubing and CuO were both pre-cleaned in the furnace at the same temperature settings prior to use. After the heating step, the purified sample gasses were introduced into the mass spectrometer by a custom-built tube cracker line operating under continuous helium flow 50 ml/min (grade 5.0). USGS61 and USGS62 reference materials were used to calibrate measured isotopic ratios to the standard delta notation relative to atmospheric air ($\delta^{15}N = [(^{15}N/^{14}N)_{sample}/(^{15}N/^{14}N)_{atmosphere} - 1] \times 1000$). USGS BHVO-2 was used as the quality control standard. Measured values for BHVO-2 of 21.0 ± 0.9 μg/g (n = 3) and a $\delta^{15}N$ value of + 2.2 ± 0.2‰ (n = 3) agree with published values (Boocock et al., 2020; 2023; Feng et al., 2018).

3.3. Bulk rock major/trace elements – XRF

Samples were analysed for major and trace element composition by energy-dispersive X-ray fluorescence (ED-XRF) on a SPECTRO XEPOS HE spectrometer at the University of St Andrews. Spectra were interpreted using fundamental parameter methods calibrated with >20 international certified reference materials. Major element abundances were measured on fused glass beads prepared by melting 0.5 g of fine sample powder with 5 g lithium borate flux (80:20 mix of Li-metaborate and Li-triborate) in platinum crucibles at 1050 °C, followed by rapid cooling in a platinum disk mould. Trace elements were measured on pressed resin powder pellets made using 4 g of fine powder mixed with 1 g of CEREOX (R) wax pressed in a 20-ton press for 30 s. Certified reference materials GSP-2 granodiorite and GS-N granite were measured to assess data quality, and the results were found to be within ±10% of expected values for all trace elements except S, Cl, V, Cr, Cs and U which had up to 30% relative errors. All major elements agreed with published values within ±0.2 wt%.

3.4. Mineral major elements – EPMA

In-situ major element data for biotite, Kspar, and plagioclase mineral phases were measured using the Cameca SX100 Electron Probe Micro Analyser (EPMA) in the Department of Earth Sciences at the University of Cambridge. For each sample, multiple mineral grains were analysed, and some were analysed for multiple points to assess inter- and intra-mineral and sample heterogeneity. An acceleration voltage of 15 kV, a beam current of 10 nA and a beam diameter of 5 μm were used. Counting times were 120 s for Ti and Ca; 40 s for Ni, Cr and Mn; 30 s for Mg and Al; 20 s for Fe and 10 s for Na, Si and K. Background counting times were set at half of the peak counting time. Secondary standards Fayalite 85276, Labradorite 115900, Omphacite 110607 and San Carlos Olivine were used to assess data quality for the measured elemental peaks. Measured values deviated from published values by <0.1 wt% for Si, Ti, Fe, Mn, Mg, Ni, K, Ca, Cr and <0.3 wt% for Al and Na. For each sample the major element average of 13–23 points for biotite and plagioclase and 4–10 points for Kspar are reported.

3.5. Mineral trace elements – LA-ICPMS

In-situ trace element data for biotite, Kspar and plagioclase were measured in the Advanced Mass Spectrometry Lab of the Earth Observatory at the University of the Witwatersrand. Samples were measured on an Australian Scientific Instruments (ASI) Applied Spectra Resolution SE193nm ArF excimer system coupled to a Thermo Fisher Scientific SF-ICP-MS system (Element XR). Spot size was set at 85 um and the laser energy was set at 7.7 mJ, resulting in a fluence of ~3.4 $J.cm^{-2}$. Laser sampling took place in an SE155 dual-volume ablation cell (Laurin Technic, Canberra, Australia) using a mixed He-Ar atmosphere and a small volume of N_2 to enhance signal stability and sensitivity. The following gas flows were applied: He = 300–400 $ml.min^{-1}$, Ar = 800–1200 $ml.min^{-1}$ and N_2 = 2–4 $ml.min^{-1}$. Data acquisition on the Element was performed in low-resolution and electrostatic scanning (E-scan) modes, using the 'triple' detector setting. The LA-ICP-MS system was tuned during line scans using NIST612 glass for maximum sensitivity for ^6Li, ^{115}In and ^{238}U, while maintaining oxide levels (ThO/Th) at <0.2%. Total signal acquisition time was 65 s, including 15 s of pre- and post-ablation (gas blank). Synthetic glass reference material NIST612 was used as the primary calibration material and ^{43}Ca EPMA data was used for internal standardisation. Mounts of glass reference materials including ATHO-G, GOR128-G, KL2-G, NIST610 and NIST614 were used to assess data quality and agreed well (within 5–15% relative error) with

published values (see Supplementary Data). Between 6 and 12 points were measured for plagioclase and biotite, and 4–10 points for Kspar, with points located on, or close to (within approximately 50–100 μm) the accompanying major element points obtained via EPMA. Data reduction was performed using Iolite.

3.6. Oxygen isotope geochemistry

Oxygen isotopes for bulk granite powders were obtained at the Scottish Universities Environmental Research Centre (SUERC) stable isotope laboratory. Around 2 mg of bulk powder were fluorinated by a laser in the presence of ClF_3 gas using established protocols (Sharp, 1990). Silicate-hosted oxygen was converted to CO_2 for isotopic measurements using a heated graphite rod. Replicate analysis of international standards UWG2 Garnet, GP147 Garnet and YP2 Quartz yielded average measured isotope ratios within 0.15‰ of accepted values and a variability of ±0.35‰ (2 s.d. around the mean). Isotope data are expressed in the conventional delta notation ($\delta^{18}O = [^{18}O/^{16}O_{sample}/^{18}O/^{16}O_{V\text{-}SMOW} - 1] \times 1000$) relative to V-SMOW. Data quality was monitored through quantitatively measuring gas yields calculated based on barometric pressure via a calibrated gas manometer. No samples were subsequently discarded for low gas yields, typically achieving yields >98%.

4. Results

Major element and Rb and N data for whole-rocks and mineral separates are shown in Table 2. Each whole-rock [N] and $\delta^{15}N$ measurement represents the average (±1 s.d.) of three replicate analyses on ca. 400 mg of bulk rock powder. Whole-rock major and trace element geochemistry shows continuous geochemical trends consistent with fractional crystallisation, such as positive slopes for incompatible elements and negative slopes for compatible elements when plotted against SiO_2 (Fig. 4). The granodiorites contain on average slightly less N (17.7 ± 2.0 μg/g, mean ± 1SD) (Fig. 5) than the granites (21.5 ± 1.7 μg/g), but they are enriched in ^{15}N (average $\delta^{15}N$ values = +8.8 ± 0.9‰ versus +4.1 ± 0.1‰, respectively). Sample LD-15 contains less N than similar granodioritic compositions with only 6.1 μg/g and shows ^{15}N-depletion relative to similar granodioritic compositions ($\delta^{15}N$ value = +3.3‰).

Bulk oxygen isotope data of the granodiorite samples are relatively ^{18}O-depleted ($\delta^{18}O$ = +7.7 ± 0.7‰) compared to the granites ($\delta^{18}O$ = +9.0 ± 0.2‰). These values are generally consistent with granitic melts

Table 2
Selected whole rock and mineral separate dataset. Nitrogen isotope values are relative to atmospheric air and oxygen isotope values are relative to V-SMOW. Errors on the N abundance and $\delta^{15}N$ values are one standard deviation. Oxygen isotope error is ±0.35‰ (2 s.d.). All N data are blank corrected. Further associated data (e.g., major and trace elements) can be found in the electronic data associated with this publication.

Sample ID	N μg/g	± ‰	$\delta^{15}N$ ‰	± ‰	Blank %	$\delta^{18}O$ ‰	Rb μg/g	SiO_2 wt.%	TiO_2 wt.%	Al_2O_3 wt.%	$Fe_2O_3^T$ wt.%	MnO wt.%	MgO wt.%	CaO wt.%	Na_2O wt.%	K_2O wt.%	LOI wt.%
WR																	
LD-19-06	17.4	1.8	+9.7	0.2	4.5	+7.8	109	61.7	1.0	15.8	5.7	0.1	4.5	3.7	3.7	3.8	1.2
LD-19-12	15.4	3.3	+8.6	0.7	5.2	+6.5	106	63.3	0.8	15.1	4.8	0.1	3.9	3.6	3.5	3.5	0.9
LD-19-13	18.4	2.4	+8.6	0.4	4.5	+7.4	116	63.4	0.7	15.4	4.5	0.1	4.1	3.2	3.3	3.7	1.0
LD-19-14	19.9	1.6	+8.0	1.3	4.0	+7.6	127	63.7	0.7	15.3	4.4	0.1	4.3	2.5	3.3	3.7	1.4
LD-19-09	17.2	3.9	+9.1	0.2	4.5	+8.4	121	63.9	0.8	15.4	5.0	0.1	4.1	3.3	3.5	3.9	1.3
LD-19-16	14.5	1.3	+8.1	1.2	5.8	+7.6	114	64.6	0.7	15.0	4.1	0.1	3.7	3.1	3.4	3.5	1.2
LD-19-08	19.7	4.8	+7.9	0.8	4.2	+7.1	120	65.5	0.7	15.2	4.4	0.1	3.9	2.7	3.6	4.0	1.1
LD-19-10	19.2	4.9	+10.4	0.8	4.6	+8.8	157	67.7	0.7	14.9	4.1	0.1	2.2	2.4	3.3	4.7	0.9
LD-19-19	22.7	3.1	+4.2	0.6	4.9	+9.2	205	71.3	0.4	13.9	2.1	0.0	1.3	1.4	3.5	4.9	0.7
LD-19-18	20.3	1.5	+4.0	0.2	4.0	+8.8	193	71.5	0.3	13.2	1.7	0.0	1.0	1.2	3.9	6.0	0.9
LD-19-15	6.1	1.9	+3.3	0.6	13.0	+8.1	106	63.9	0.7	15.0	4.4	0.1	3.7	3.7	3.8	3.4	0.9
Biotite																	
LD-19-06	11.1	2.2	+3.9	1.4	10.2	+6.2	391	39.1	4.2	14.3	18.4	0.2	13.5	0.1	0.2	10.1	
LD-19-12	10.7	2.1	+0.6	1.4	18.3			39.1	4.1	13.9	18.6	0.2	13.8	0.1	0.1	10.1	
LD-19-13	11	2.2	+1.8	1.4	12.6		447	39.2	4.1	14.0	18.2	0.2	13.9	0.1	0.1	10.1	
LD-19-14	9.9	2	+2.5	1.4	14.0		402	39.1	3.9	14.3	18.0	0.2	14.2	0.1	0.2	9.9	
LD-19-09	13.5	2.7	+2.8	1.4	7.8		488	39.1	4.1	14.0	18.2	0.2	13.9	0.1	0.1	10.1	
LD-19-16							475	39.1	4.0	14.0	18.3	0.2	13.9	0.1	0.1	10.1	
LD-19-08	12.7	2.5	+2.6	1.4	10.8	+5.1	468	39.0	4.1	14.1	18.4	0.2	13.8	0.1	0.1	10.1	
LD-19-10						+6.9	679	38.7	4.4	14.1	20.4	0.4	11.8	0.1	0.1	10.1	
LD-19-19	21.9	4.4	−5.3	1.4	5.9	+5.0	899	38.8	4.5	13.6	20.1	0.4	12.3		0.1	10.2	
LD-19-18	23.8	4.8	−3.8	1.4	5.6		731	39.0	4.2	14.1	20.1	0.4	12.2	0.1	0.1	9.9	
Plag																	
LD-19-06	19.2	2.5	+9.4	0.6	4.8	+8.8	60	58.6		25.9	0.2			7.9	7.3	0.3	
LD-19-12	19.8	2.6	+9.5	0.6	3.7		169	59.9		24.8	0.2		0.2	6.8	8.0	0.3	
LD-19-13	23.2	3	+9.7	0.6	3.0		155	60.4		24.7	0.2			6.5	8.0	0.3	
LD-19-14	13.3	1.7	+9.6	0.6	5.3		251	65.8		21.1	0.3		0.1	1.9	10.7	0.4	
LD-19-09	14.6	1.9	+11.8	0.6	5.4		149	61.2		24.0	0.2			5.8	8.6	0.3	
LD-19-16							148	60.0		24.7	0.2		0.1	6.8	8.1	0.3	
LD-19-08	17.9	2.3	+10.0	0.6	4.5	+8.3	147	62.5		23.3	0.2		0.1	4.4	9.1	0.5	
LD-19-10						+11.8	58	60.8		24.3				6.2	8.4	0.3	
LD-19-19	9.6	1.2	+3.2	0.6	7.7	+9.0	80	62.4		23.4	0.1		0.1	4.7	9.1	0.3	
LD-19-18	8.4	1.1	+4.3	0.6	5.0		32	61.5		24.1	0.1			5.6	8.4	0.3	
Kspar																	
LD-19-06	33.7	3.7	+11	0.8	2.3			65.2		18.4					1.2	15.3	
LD-19-12	32.2	3.5	+9.0	0.8	2.3		185	64.6		18.8	0.2				1.5	15.1	
LD-19-13	31.7	3.5	+10.6	0.8	2.3		171	65.0		18.5					1.3	15.2	
LD-19-14	38.6	4.2	+9.2	0.8	1.7		378	64.8		18.8				0.4	1.8	14.6	
LD-19-09	36.8	4	+10.4	0.8	2.1			64.5		18.7				0.2	0.9	15.9	
LD-19-16							235	64.7		18.5				0.1	1.3	15.6	
LD-19-08	38.2	4.2	+9.7	0.8	2.0		205	64.7		18.6	0.1				0.9	16.0	
LD-19-10							235	64.7		18.2	0.9			0.1	0.9	15.9	
LD-19-19	46.1	5.1	+4.2	0.8	2.0		456	64.7		18.3				0.2	1.1	15.9	
LD-19-18	45.2	5	+4.1	0.8	2.0		428	64.6		18.2	0.1			0.2	1.1	15.7	

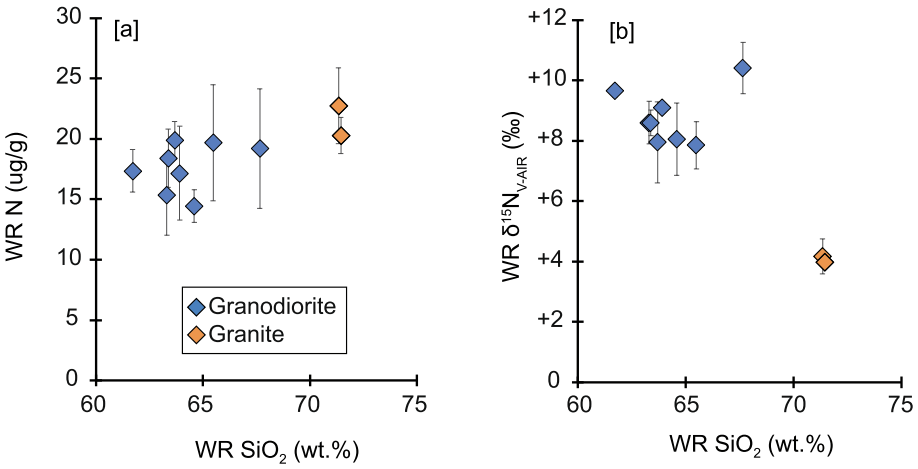

Fig. 5. Whole rock N data. Coloured according to compositional classifications. Errors represent one standard deviation on the mean of replicate analyses.

formed with the incorporation of crustal materials either during emplacement or from a subducted source (Bindeman, 2008). A limited number of mineral-specific $\delta^{18}O$ values were obtained (Table S1).

For eight samples, mineral separates of Kspar, plagioclase, and biotite (and for three samples, quartz) were hand-picked and measured for N abundances and $\delta^{15}N$ values (Table 2). Nitrogen abundances are highest in the Kspar separates (31.7–46.1 μg/g) for both granodioritic and granitic compositions. In the granodioritic compositions, plagioclase held the next highest amount of N (13.3–23.2 μg/g), followed by biotite (9.9–13.5 μg/g). But in the granitic compositions, biotite held more N (21.9–23.8 μg/g) than plagioclase (8.4–9.6 μg/g). The three aliquots of quartz were consistently depleted in N (average 2.8 μg/g, not shown in Table 2), as expected, which provides indirect support for our efforts of removing all N contamination because the quartz shows near blank levels of N. Overall, we find that N partitions more strongly into feldspars over biotite in this system. Mass balance calculations, accounting for the modal abundances of minerals, show that within the granodiorites 19–34% (average 29%) of the N is hosted in the Kspar, 27–58% (average 42%) is hosted in the plagioclase, and 5–15% (average 10%) is hosted in the biotite. Note, our plagioclases are not K-free and contain a minor orthoclase component (Or_{1-3}). The remaining 2–34% (average 19%) of the N is hosted in unmeasured mineral phases (presumably actinolite or pyroxene). In the granites, 57–65% (average 61%) of the N is hosted in the Kspar, 12–13% (average 13%) is hosted in the plagioclase, 6% is hosted in the biotite, and 17–24% (average 20%) is hosted in unmeasured mineral phases (presumably cordierite). The data for the three quartz mineral separates (from samples LD06, LD09, LD19, Table S1) have relatively large blank contributions (60% of the measured signal), making them imprecise. They are therefore not included in the mass balance calculation. However, they confirm that quartz is not a significant host for the remaining N in this system. This agrees with previous measurements showing that primary magmatic quartz hosts little-to-no detectable N (Honma and Itihara, 1981).

5. Discussion

5.1. Alteration

Determining whether hydrothermal alteration or weathering has added or removed N post crystallisation of these samples is critical to ensure we are viewing data reflecting magmatic processes. The hand specimens of these samples appear fresh with no macroscopic optical evidence of alteration. However, on the microscopic scale, sericitization of the feldspars (plagioclase and Kspar) is observable (Fig. 2). We examined the effect of the sericitization on sample geochemistry and found no evidence for alteration effects on fluid-mobile elements (Ca, K, Ba, Sr, N). For example, the whole-rock loss on ignition (LOI) values are low, ranging from 0.73 to 1.41% (av. 1.04 ± 0.2%; Table 2), consistent with the loss of OH^- component of biotite and minor sericite (proportionally) but inconsistent with abundant secondary clay minerals. In addition, weak correlations are found for whole-rock LOI versus CaO ($R^2 = 0.1$), K_2O ($R^2 = 0.2$), Ba ($R^2 = 0.6$), Sr ($R^2 = 0.5$), N ($R^2 = 0.0005$), $\delta^{18}O$ values ($R^2 = 0.2$) and $\delta^{15}N$ values ($R^2 = 0.1$). Furthermore, whole-rock (i.e., including igneous minerals and minor sericitization phases) Sr and Rb abundances correlate positively with LA-ICP-MS measurements for Sr in un-sericitized sections of plagioclase ($R^2 = 0.7$), and Rb in un-sericitized sections of Kspar ($R^2 = 0.7$) and for biotite ($R^2 = 0.9$). To examine this further, we consider the concentration of key fluid mobile elements (NH_4, Rb, and Ba) in biotite and Kspar. Nitrogen correlates well with Rb in Kspar and biotite (Fig. 6), which is explained by the preference for NH_4^+ to follow the partitioning behaviour of Rb^+ during crystal growth from a silicate melt (R^2 = 0.9 and 0.8 respectively). However, N contents of Kspar and biotite show poor correlation coefficients with the corresponding Ba content in the same phases (R^2 = 0.4 and 0.1 respectively). Collectively, and despite the sericitization of the feldspars (plagioclase and Kspar) observed in the thin sections (Fig. 2), these data indicate that the abundances of LILE and N in the

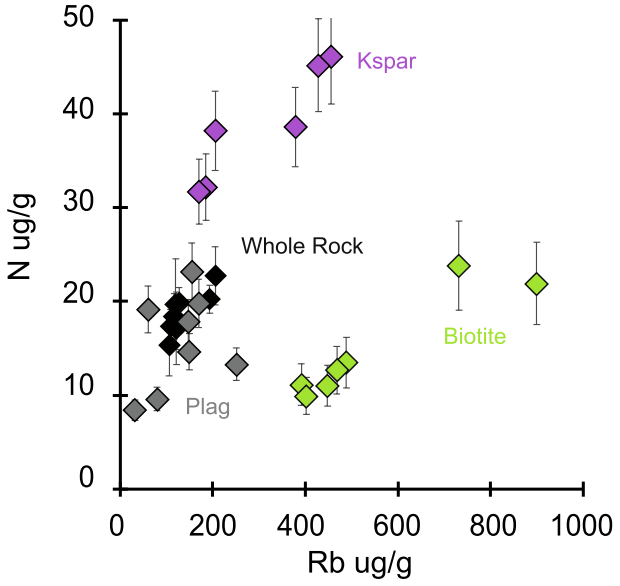

Fig. 6. Nitrogen versus Rb for mineral separates and whole rock. The difference between biotite being lower in N and high in Rb relative to Kspar indicates a decoupling of N and Rb.

Kspar and biotite were controlled and set by primary igneous processes in these samples.

5.2. Source of nitrogen

At a whole-rock scale, N abundances are relatively homogenous across the sample suite with a narrow range from 14.5 to 22.7 μg/g (Table 2) and poor correlation with whole-rock SiO_2 ($R^2 = 0.47$). We do, however, observe a difference between the average $\delta^{15}N$ values of granodiorites (average $\delta^{15}N = +8.8 \pm 0.9‰$) and granites (average $\delta^{15}N = +4.1 \pm 0.1‰$), which is consistent with data from other isotope systems in the Loch Doon magmatic system (e.g., Sr, Nd, O; Hines et al., 2018). It is conceivable that the dioritic and granitic melts represent pulses of different magmas, a notion which – if the case – would not infringe upon the findings of this study because the aim is to investigate elemental partitioning and stable isotope fractionation of N between biotite, plagioclase, and Kspar relative to each other within their respective systems (whole rocks). Section 5.1 explains why we consider the abundances of LILE and N in the Kspar and biotite to be controlled and set by primary igneous processes in these samples, meaning that the source of N still needs to be considered. There are two options, assimilation of nitrogen into a magma from country rock at a high crustal level or primary derivation from the melt source region (e.g., subducted crustal N). To homogenise N between minerals and melt at a pluton scale would require diffusion below 800 °C (i.e., below the crystallization temperature) to be more rapid than determined in experiments. For example, Yang et al (2022) show that for temperatures > 800 °C, most N should be retained in feldspar structure until the breakdown of feldspar (either melting or phase transition to spinel or garnet). Moreover, it has been shown that N diffusion through Kspar over 100 mm requires 1 Gyr at 800 °C (Watson et al., 2019). Therefore, full equilibration on the scale of an outcrop or pluton via volume diffusion is impossible because the Loch Doon pluton was emplaced 408 ± 2 million years ago (Halliday et al., 1978). We also observe no change in N abundances towards the margin of the pluton, which would be expected if the N in the Loch Doon pluton were sourced from the surrounding country rock(s) via syn- or post-emplacement assimilation. Therefore, the N hosted in these igneous minerals is most likely reflective of their magmatic source.

The average $\delta^{15}N$ values of granodiorites (average $\delta^{15}N = +8.8 \pm 0.9‰$) and granites (average $\delta^{15}N = +4.1 \pm 0.1‰$; Table 2) are distinct from the ambient upper mantle ($\delta^{15}N = -5 \pm 3‰$; Mikhail et al., 2014), ruling out a pure mantle source for N at Loch Doon. Similarly, the local country rock (represented by our sample LD-04, $\delta^{15}N = +1.3 \pm 0.5‰$ (n = 1), and the Moffatt Shale Group, $\delta^{15}N = +1.0 \pm 0.4‰$ (n = 31; Koehler et al., 2019) are too ^{15}N-depleted to account for the bulk $\delta^{15}N$ signatures of this pluton. Simple binary mixing between greywacke/shale and mantle does not produce the whole-rock N signatures for the Loch Doon granodiorites or granites (Fig. 7a). Note that these sediments are a part of the Iapetus accretionary prism, therefore can be considered to be roughly contemporaneous to the sedimentary cover that was subducted and ultimately melted to produce the granitic magmatism which Loch Doon is a part of. Since this high crustal level mixing cannot produce the measured whole-rock signatures, we consider the impact of subduction on the sediment-derived N endmember (Miles et al., 2016). Taking the local greywacke and shale compositions from above, we can model the impact of increasing metamorphic devolatilization on these

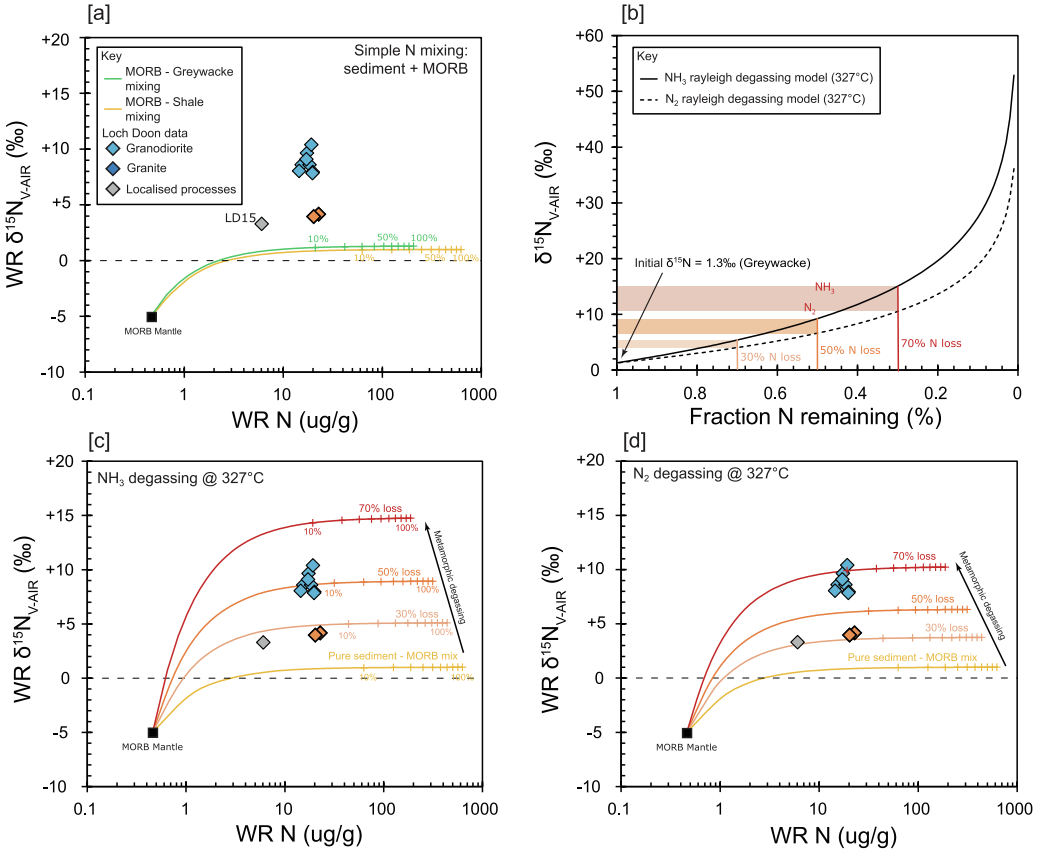

Fig. 7. (a) binary mixing diagram of MORB mantle (Cartigny et al., 2014) and local greywackes (This study – LD04) and shales (Koehler et al., 2019). (b) $\delta^{15}N$ Rayleigh devolatilization model of local sediments to model effect of increasing metamorphism during subduction, used to estimate a number of "subducted sediment" endmembers for mixing models in c and d. (c) Mixing diagram between mantle and a number of hypothetical "subducted sediment" endmembers for NH_3 degassing at 327 °C (600 K). (d) mixing diagram between mantle and a number of hypothetical "subducted sediment" endmembers for N_2 degassing at 327 °C (600 K).

sediments (Fig. 7b), utilising empirical fractionation factors (for metamorphic devolatilization) derived from a suite of progressively devolatilised metasediments (Haendel et al. (1986). These models are purely illustrative, but they demonstrate that subduction of sediments similar in composition to the surrounding accretionary prism can theoretically produce an endmember for isotope mixing with the mantle which may explain the meausred whole-rock N signatures of Loch Doon. In brief, as subduction-driven devolatilization progresses, the residual rock is progressively enriched in ^{15}N (Fig. 7b). We modelled both the result of loss as NH_3 and N_2; however, the low concentrations of N trapped in the three quartz separates could suggest that the N in the K-phases is mostly speciated as NH_4^+, because N speciated as fluid-dissolved N_2 would be expected to be trapped in inclusions in the quartz as much as in other mineral phases. Estimates for the percentage loss of N during subduction are highly variable from 8 to 100% (e.g., Busigny et al., 2011; Elkins et al., 2006; Förster et al., 2019; Fischer et al., 2002), so we chose three scenarios with 30%, 50% and 70% loss of N (Fig. 6c, 6d). In general, loss as NH_3 (Fig. 7c) yields endmember compositions with higher $\delta^{15}N$ values than the loss of N_2 (Fig. 7d). These calculations assume a temperature of 327 °C (600 K) as an example of feasibility. If we use fractionation factors for higher temperatures (e.g., 527 or 727 °C), the calculated value for the modelled subducted sediment $\delta^{15}N$ endmember is lower, and therefore higher percentages of devolatilization would be required. These illustrative models show that mixing between a mantle component ($\delta^{15}N = -5 \pm 3$‰; Mikhail et al., 2014) and a sedimentary component that has undergone a degree of subduction-driven devolatilization can generate a trend which traverses through – but cannot fit – the $\delta^{15}N$-[N] data observed at Loch Doon (Fig. 7). As such at a whole-rock scale, our data seem to best match a scenario where the melt inherited its N signatures from a subducted sedimentary source rather than high level crustal assimilation post emplacement.

5.3. Elemental partitioning of nitrogen during magmatic differentiation

We have so far shown evidence that the N in the Loch Doon pluton is likely of primary magmatic origin (Sections 5.1 and 5.2). Therefore, we can use these data to assess the partitioning behaviour of nitrogen in this system as representative of N partitioning during magmatic processes. To our knowledge, there is only one other study to date which looks systematically at inter-mineral partitioning in natural igneous systems (Honma and Itihara (1981), although other studies do exist for metamorphic lithologies and experimental samples. We compare the N geochemistry of Kspar, plag, and biotite to whole rock, determine the proportion of N hosted by these mineral phases in each unit of the zoned pluton sampled in this study (Table 3; Fig. 8a-b), and discuss these data in light of complimentary work from the literature.

Previous work on gneissic granodiorites and granites from the Ryoke belt in Japan by Honma and Itihara (1981) found that N partitioned in the order of biotite > muscovite ≈ Kspar > plagioclase > quartz. These data have since been widely used as evidence that the presence of biotite is a controlling influence over the distribution of N in magmatic systems (e.g., Busigny and Bebout, 2013; Johnson and Goldblatt, 2015). However, at Loch Doon, we observe N partitioning in the order of that Kspar > plagioclase ≈ biotite > quartz (Table 3). Importantly, we find that N is preferentially hosted by Kspar, regardless of bulk composition (Fig. 8a-b).

Relative to the whole rock, we find that the average N content of the plagioclase separates equates to the whole rock, biotite is marginally depleted, with N dominantly hosted by Kspar ($D_{N\ Kspar\text{-}wholerock} = 2.0 \pm 0.2$) (Table 3; Fig. 8a-b). We have calculated distribution coefficients for N between Kspar and biotite, which yield average D values of 2.8 ± 0.6 in favour of Kspar (Table 3 & Fig. 8a-b). These results agree well with experimental and natural data from other studies with similar bulk compositions (e.g., all intermediate to high-Si rocks) for both K and Rb (Table 4). Our biotite-to-whole-rock N data also closely match published biotite-melt values (Förster et al., 2019; Jackson et al., 2021). However, our N data contrast with recent experimental Kspar-melt data from Jackson et al., (2021; Table 3). There are two likely reasons for the disagreement: [1] a potential source of this discrepancy may be the nature of the plutons, where whole-rock pluton compositions do not represent melt compositions, and [2] analytical uncertainties may be too large (at present an unavoidable consequence of the small sample sizes in HPHT experiments for N using EMPA). However, it is not possible to distinguish between these possibilities (and they are not mutually exclusive).

For the granodioritic samples, N is marginally enriched in plagioclase over biotite ($D_{N\ plagioclase\text{-}biotite} = 1.6 \pm 0.4$), which is in contrast with the previous study by Honma and Itihara (1981). We note that our plagioclase compositions are more sodic ($Ab_{60\text{-}75}$) than the plagioclase measured in Honma and Itihara (1981) ($Ab_{<60}$), and those at Loch Doon contain a small orthoclase component ($plag_{99\text{-}97}$–$Or_{1\text{-}3}$). Busigny et al. (2011) suggested NH_4^+ can partition into Ca-Na bearing minerals in metagabbro, where K^+ is limited, and proposed that NH_4^+ can substitute for Na^+. Although our system contains significant K^+, we still observe a preference for NH_4^+ partitioning into sodic minerals ($plag_{99\text{-}97}$–$Or_{1\text{-}3}$) over biotite. A shift occurs in the granitic compositions where N compatibility in plagioclase drops ($D_{N\ plagioclase\text{-}biotite} = 0.4 \pm 0.1$), but Kspar remains the preferred host with a negligible change in relative distribution coefficients ($D_{N\ Kspar\text{-}wholerock} = 2.1 \pm 0.1$ and $D_{N\ Kspar\text{-}biotite} = 2.0 \pm 0.1$; Fig. 8a-b).

We observe a coupling between N and Rb during magmatic differentiation (Fig. 6), which is expected based on what has been observed in a suite of cogenetic and aphyric volcanic samples (Boocock et al., 2023). However, in this study we observe a decoupling of N from Rb where Kspar and biotite coexist (note, Kspar is not present in Hekla lavas; Boocock et al., 2023). For Loch Doon, we find that N is significantly more compatible in Kspar than Rb, while the opposite is true for biotite (Fig. 6). This implies that the assumption where the ammonium ion is similar in size to Rb^+ and therefore partitioning between N and Rb should be proportional, is incorrect. Our data support the possibility that the size of the ammonium ion is smaller than Rb^+, because in Kspar the K-site site is smaller than for biotite and enables the accommodation of smaller ions. Conversely, these data open the possibility that there are no universally applicable D values for N in igneous systems, where equilibrium exchange coefficients between different host phases (with different solid-solutions) might be more useful to express the behaviour of N in a given system with >1 K-bearing phase.

5.4. Isotopic fractionation of nitrogen during magmatic differentiation

Despite the significant difference in the distribution coefficients for N between plagioclase and Kspar (Fig. 8a-b & Table 3), when considering the uncertainties, we find no isotopic difference between the two

Table 3
Measured mineral-whole rock and mineral–mineral distribution coefficients and stable isotope fractionation factors for N in all samples, granites, and granodiorites samples at Loch Doon.

	All		Granite		Granodiorite	
	D_N	σ	D_N	σ	D_N	σ
Kspar-WR	2	0.2	2.1	0.1	2	1.4
Plag-WR	0.9	0.3	0.4	0	1	0.2
Biotite-WR	0.8	0.2	1.1	0.1	0.6	0.1
Kspar-Plag	2.8	1.5	5.1	0.4	2.1	0.6
Plag-Biotite	1.3	0.6	0.4	0.1	1.6	0.4
Kspar-Biotite	2.8	0.6	2	0.1	3.1	0.4
	$\Delta^{15}N$ (‰)	σ	$\Delta^{15}N$ (‰)	σ	$\Delta^{15}N$ (‰)	σ
Kspar-WR	1	0.8	0.1	0.1	1.4	0.6
Plag-WR	0.9	1.2	−0.3	0.9	1.4	0.1
Biotite-WR	−6.8	1.5	−8.6	1.2	−6.3	1
Kspar-Plag	0.1	1	0.4	0.8	0	1.1
Plag-Biotite	7.8	1.2	8.3	0.3	7.6	1.3
Kspar-Biotite	7.9	1	8.7	1.1	7.6	0.8

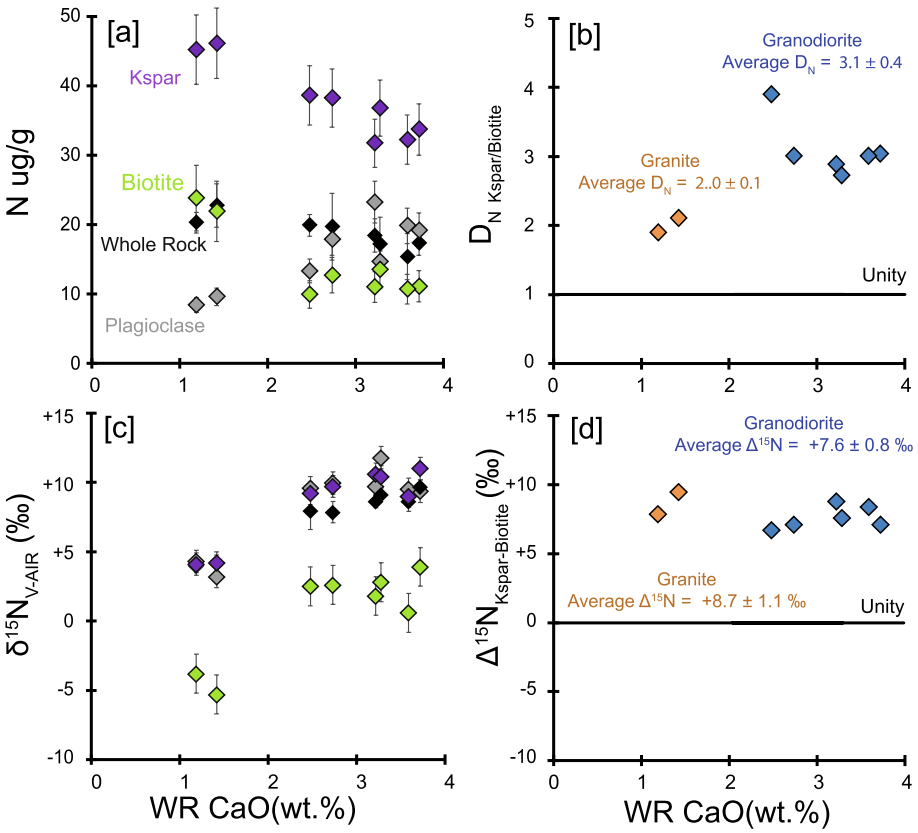

Fig. 8. Selected plots to illustrate key findings in this study. Whole rock CaO is plotted on the x-axis because our samples span a narrow range of SiO_2 (granodiorite-granite). [a] The N content of mineral separates vs CaO shows that N is preferentially hosted in Kspar, regardless of bulk composition. [b] shows $D_{N\ Kspar\text{-}biotite}$ is >1 regardless of bulk composition but does show variability as a function of WR CaO. [c] shows $\delta^{15}N$ vs CaO which demonstrates that there is a decrease in the WR $\delta^{15}N$ value as the system evolves from granodiorite-granite, where biotite is constantly 15 N-deplted retaliative to Kspar, Plag, and WR. [d] illustrates the strong isotope effect where $\Delta^{15}N_{Kspar\text{-}Biotite} = +7.9 \pm 1.0‰ =$, regardless of N content, WR composition, and WR or mineral specific $\delta^{15}N$ value.

Table 4
Measured mineral-whole rock partition coefficients versus published mineral-melt partition coefficients from the literature (Bea et al., 1994; Förster et al., 2019; Higuchi and Nagasawa, 1969; Icenhower and London, 1996; Jackson et al., 2021; Nagasawa and Schnetzler, 1971; Nash and Crecraft, 1985; Philpotts and Schnetzler, 1970).

	This study		Source literature>	Förster et al. (2019)	Jackson et al. (2021)	Bea et al. (1994)	Nash & Crecraft (1985)	Icenhower and London (1996)	Philpotts and Schnetzler (1970)	Higuchi and Nagasawa (1969)	Nagasawa and Schnetzler (1971)
	All Samples	Σ	**Lithology >**	experimental	experimental	peraluminous granites	rhyolites	rhyolites	dacites	dacites	dacites
D_N			D_N								
Kspar-WR	2.0	0.2	Kspar-melt		0.15–0.4						
Plag-WR	0.9	0.3	Plag-melt								
Biotite-WR	0.8	0.2	Biotite-melt	0.4–1.2	0.5–0.7						
D_{Rb}			D_{Rb}								
Kspar-WR	2.1	0.5	Kspar-melt			2.9	1.2–2.4				
Plag-WR	1.1	0.6	Plag-melt			0.1					
Biotite-WR	3.8	0.4	Biotite-melt			7.0	2.3–4.1				
D_K			D_K								
Kspar-WR	3.8	0.6	Kspar-melt					0.3–3.1			
Plag-WR	0.1	0	Plag-melt								<0.1
Biotite-WR	2.5	0.4	Biotite-melt						2.6–5.6	2.5	

feldspars (average $\Delta^{15}N_{Kspar\text{-}Plag} = 0.2 \pm 1.0‰$, Table 3). We do, however, find a significant and near constant isotopic offset between biotite and both feldspar types across the full differentiation range, and lithological rock types ($\Delta^{15}N_{Plag\text{-}Biotite} = +7.8 \pm 12‰$ and $\Delta^{15}N_{Kspar\text{-}Biotite} = +7.9 \pm 1.0‰$; Fig. 8c-d & Table 3). These $\Delta^{15}N_{Kspar\text{-}Biotite}$ and $\Delta^{15}N_{Plag\text{-}Biotite}$ fractionation factors are larger than current estimates obtained via density functional theory (DFT) simulations ($10^3 ln\beta = +0.5‰$ at 700 °C, where $10^3 ln\beta \approx \Delta^{15}N$; Li et al., 2021). At first glance, this discrepancy may suggest the biotite grains are not at magmatic equilibrium, consistent with similar ^{15}N depletion observed in

hydrothermal biotite (Li et al., 2014). However, petrological (little to no signs of chloritization, euhedral crystal morphology, primocrystic textures – Fig. 3) and geochemical lines of evidence (high Ti contents of 4 to 4.5 wt% due to the increase in Ti solubility in biotite at magmatically relevant high temperatures; Robert, 1976) suggest that the biotite crystals in our samples are fresh and magmatic in origin with limited secondary alteration. The constancy of $\Delta^{15}N$ implies limited temperature variability, and using the Ti content in biotite as a geothermometer (Henry et al., 2005), we calculate a temperature range for biotite crystallisation from 784 °C to 794 °C across the whole sample suite. The direction of $\Delta^{15}N_{Plag\text{-}Biotite}$ and $\Delta^{15}N_{Kspar\text{-}Biotite}$ is expected, because heavier isotopes prefer stronger bonds (Urey, 1947). Bond strength is determined by a combination of bond length, coordination number, ionic charge, and valence state. If we assume that the main partitioning species is NH_4^+ (Busigny and Bebout, 2013), as supported by the near-absence of N in quartz, then mineral sites with lower coordination numbers and shorter bond lengths should favour ^{15}N over ^{14}N. Assuming that NH_4^+ substitutes for K^+ in mica and feldspar, the K-O bond length and coordination in these minerals would dictate the direction and magnitude of equilibrium isotopic fractionation. In feldspars, the average K-O bond coordination and length decrease with K concentration (Downs et al., 1996), with longer bonds in the potassic felspar microcline (~2.92 Å) and shorter bonds in Na-rich albite (~2.80–2.63 Å). This is accompanied by a small reduction in coordination number from 7 in microcline to 5 in albite (Downs et al., 1996). By contrast, biotite has longer K-O bond lengths (~2.99 Å) and a much larger difference in coordination number (7 to 11) (Cibin et al., 2005). Based on these variables, one would expect the feldspars to be ^{15}N-enriched relative to the biotite (as is found in this study), and agreeably estimated (in direction) by theoretical calculations for the equilibrium N isotope fractionation (Li et al., 2021). One reason why our empirical inter-mineral N isotope fractionation factors may be larger than the theoretical calculations may be due to differences in the chemical composition of their idealised mica formula versus our naturally occurring biotite. Natural minerals tend to have a variety of trace element imperfections. Imperfections in the mineral lattice would lead to structural distortions, which would impact the natural bond length and coordination numbers. This has previously been shown to be an issue for comparing natural Kspar-mica K isotope fractionation (Huang et al., 2023) compared with theoretical DFT calculations (Li et al., 2019), where Huang et al. (2023) found a larger isotope fractionation factor between natural mica and feldspar than predicted by DFT. The discrepancy was attributed to differences in perfect mica structure K-coordination numbers (ca. 6) used in the DFT calculations vs. natural mica K-coordination numbers (ca. 7–11). In addition, we stress that $\Delta^{15}N$ values may differ in systems where N dissolved in the silicate melt is not only speciated as NH_4^+ (Li and Keppler, 2014; Mikhail et al., 2017; Mikhail and Sverjensky, 2014). Changes in the oxidation state of N (e.g., NH_4^+, NH_3, NH_2^-, N_2, N^{3-}) will result in differences in bonding energy and coordination number and could drive redox-sensitive isotopic fractionation as seen with other redox sensitive elements (Schauble, 2004). Note, we do not rule out mineral–mineral $^{15}N/^{14}N$ equilibration, but we also leave open the possibility that the $^{15}N/^{14}N$ equilibrium occurred between Kspar-melt and biotite-melt, where the speciation of N in the mineral is NH_4^+ while the speciation in the melt is less well constrained and may not be mono-speciated. In any case, we observe consistency for our calculated $\Delta^{15}N_{Kspar\text{-}Biotite}$ (Fig. 8d), even though the WR $\delta^{15}N$ values for granodiorite and granite differ (+8.8 ± 0.9‰ vs. +4.1 ± 0.1‰; Table 2; Fig. 8c). When combined with petrographic, major and trace element evidence for approximately closed system fractionation, we posit that this evidence supports the notion that we have recorded an equilibrium N stable isotope fractionation effect.

5.5. Implications

Our data represent the first combined N abundance and isotope ratio measurements of coexisting magmatic phases during plutonic differentiation. A key finding of this study is that N preferentially partitions into Kspar over biotite, which contrasts with previous data (Honma and Itihara, 1981). The implications of these data are that feldspars need closer scrutiny with regards to cycling of N in the geosphere. If feldspars are a significant host for N in plutonic rocks, then this has key implications for quantifications of the N weathering flux. Feldspar breakdown to secondary clay minerals during weathering (Yuan et al., 2019) would release silicate bound NH_4^+ as a leachable solute into soils, rivers, and oceans (as is the case for Ca^{2+}, K^+, and Na^+). In groundwater systems, the activity of reactive N can be a biologically limiting factor (Rogers et al., 1998), and therefore identifying a new abiotic process to provide reactive N may shed light on an important link between the geological, climatic, and biological N cycles.

Another implication is that the significance of plagioclase feldspar in mafic and intermediate compositions may be worth reassessing. We find greater compatibility in plagioclase than expected if N were partitioning akin to K and Rb. This finding suggests a favourable substitution between N and Na as previously tabled (Busigny et al., 2011), although there is a 1–3% orthoclase component in Loch Doon plagioclase crystals, which may permit the incorporation of N as NH_4^+ substituting for K^+. If plagioclase does indeed host equal amounts of N to biotite in intermediate magmatic systems, then plagioclase might be a globally significant N host in settings such as subducting oceanic crust, differentiating lavas, mafic to intermediate plutonic systems, and the entirety of the igneous portion of Earth's oceanic and upper continental crust.

6. Conclusions

We show that bulk rock N abundances and $\delta^{15}N$ values are inherited features of the source composition at Loch Doon. We find that a mixture of mantle-derived and subducted sedimentary N can be evoked to explain the whole-rock N signatures. This signature cannot be inherited via high-level crustal assimilation following pluton emplacement, as this would result in a more significant intra-sample heterogeneity on a pluton scale and fails to satisfy the high and homogenous whole-rock $\delta^{15}N$ values.

Secondly, we find that magmatic partitioning of N into common felsic minerals show a preference in the order Kspar > plagioclase ≈ biotite > quartz. Generally, N follows a similar partitioning behaviour to Rb in the feldspars but shows a decoupling from Rb in biotite. This may arise due to differences in the bonding environments between minerals and/or differing abilities to incorporate multiple species of N. Our data imply that where Kspar and biotite coexist in intermediate to evolved igneous systems, that Kspar dominates the N budget.

Finally, we find that magmatic differentiation imparts consistent and significant N stable isotope fractionation. The consistency for our calculated $\Delta^{15}N_{Kspar\text{-}Biotite}$, where the, $\delta^{15}N$ values for both phases vary as the plutonic system evolves from intermediate to silicic, suggests that we have recorded equilibrium stable isotope fractionation factors. We find that whole-rock $\delta^{15}N$ is dominantly preserved by feldspars and that both Kspar and plagioclase are minimally isotopically fractionated relative to one another. By contrast, biotite shows a large consistent negative isotopic offset relative to the feldspars (average $\Delta^{15}N_{Biotite\text{-}Kspar} = -7.9 \pm 1.0$‰) and the whole rock (average $\Delta^{15}N_{Biotite\text{-}WR} = -6.8 \pm 1.5$‰).

In summary, feldspars might be a globally significant N host in settings such as subducting oceanic crust, differentiating lavas, mafic to intermediate plutonic systems, and the entirety of the igneous portion of Earth's continental and oceanic crust. As such, incongruent weathering of mica and feldspars should be considered as a source of isotopically heterogeneous N to surface environments, where it may serve as a nutrient to the biosphere in the present and the deepest past.

Declaration of Competing Interest

The authors declare that they have no known competing financial interests or personal relationships that could have appeared to influence the work reported in this paper.

Acknowledgements

We thank Stuart Allison and Sebastian Fischer at the University of St Andrews for technical support during thin section production and XRF measurements. We would also like to thank Alison McDonald, SUERC, for their support during collection of the oxygen isotope data. We acknowledge funding from a NERC studentship (to TJB; NE/R012253/1), a National Environmental Isotope Facilities grant (to EES, SM, and TJB; NEIF – 2313.0920), a NERC Frontiers grant (to EES; NE/V010824/1) and a NERC standard grant (to SM; NE/PO12167/1). We are grateful to Long Li (Univ. Alberta) and one anonymous reviewer for their rigorous and constructive feedback, and to the editorial work of handling editor Ralf Halama.

Author contributions

SM, EES, and JP developed the idea. TJB, SM and EES drafted the manuscript with input from RK, AJB, JP and GB. TJB, RK and SM collected the samples. TJB and RK prepared the samples. TJB collected the N data, TJB and RK performed XRF measurements, TJB and IB performed EPMA measurements. TJB and AJB collected the O data. GB collected the LA-ICPMS trace element data.

Appendix A. Supplementary material

Supplementary data is an Excel (xlsx.) spreadsheet with two tabs. Tab 1 is all the data generated in this study, and tab 2 is a fully referenced data compilation from the literature. Supplementary material to this article can be found online at https://doi.org/10.1016/j.gca.2023.07.010.

References

Ahadnejad, V., Hirt, A., Valizadeh, M., Bokani, S., 2011. The ammonium content in the Malayer igneous and metamorphic rocks (Sanandaj-Sirjan Zone, Western Iran). Geol. Carpathica 62, 171–180.
Bamford, D., Nunn, K., Prodehl, C., Jacob, B., 1978. LISPB – IV. Crustal structure of Northern Britain. Geophys. J. Int. 54, 43–60.
Barry, P.H., Hilton, D.R., 2016. Release of subducted sedimentary nitrogen throughout Earth's mantle. Geochem. Perspect. Lett. 2, 148–159.
Bea, F., Pereira, M.D., Corretge, L.G., Fershtater, G.B., 1994. Differentiation of strongly peraluminous, perphosphorus granites: The pedrobernardo pluton, central Spain. Geochim. Cosmochim. Acta 58, 2609–2627.
Bebout, G.E., Fogel, M.L., 1992. Nitrogen-isotope compositions of metasedimentary rocks in the Catalina Schist, California: Implications for metamorphic devolatilization history. Geochim. Cosmochim. Acta 56, 2839–2849.
Bebout, G.E., Cooper, D.C., Don Bradley, A., Sadofsky, S.J., 1999. Nitrogen-isotope record of fluid-rock interactions in the Skiddaw aureole and granite, English Lake District. Am. Mineral. 84, 1495–1505.
Bindeman, I., 2008. Oxygen isotopes in mantle and crustal magmas as revealed by single crystal analysis. Rev. Mineral. Geochem. 69, 445–478.
Boocock, T.J., Mikhail, S., Prytulak, J., Di Rocco, T., Stueken, E.E., Stüeken, E.E., 2020. Nitrogen mass fraction and stable isotope ratios for fourteen geological reference materials: evaluating the applicability of elemental analyser versus sealed tube combustion methods. Geostand. Geoanalytical Res. 44, 537–551.
Boocock, T.J., Mikhail, S., Adrian, B.J., Prytulak, J., Savage, P.S., Stüeken, E.E., 2023. A primary magmatic source of nitrogen to Earth's crust. Nat. Geosci. 16, 521–526.
Boyd, S.R., 1997. Determination of the ammonium content of potassic rocks and minerals by capacitance manometry: a prelude to the calibration of FTIR microscopes. Chem. Geol. 137, 57–66.
Boyd, S.R., Hall, A., Pillinger, C.T., 1993. The measurement of $\delta^{15}N$ in crustal rocks by static vacuum mass spectrometry: Application to the origin of the ammonium in the Cornubian batholith, southwest England. Geochim. Cosmochim. Acta 57, 1339–1347.
Brown, G.C., Cassidy, J., Tindle, A.G., Hughes, D.J., 1979. The Loch Doon granite: an example of granite petrogenesis in the British Caledonides. J. Geol. Soc. London. 136, 745–753.
Busigny, V., Bebout, G.E., 2013. Nitrogen in the silicate Earth: Speciation and isotopic behavior during mineral-fluid interactions. Elements 9, 353–358.
Busigny, V., Cartigny, P., Philippot, P., Ader, M., Javoy, M., 2003. Massive recycling of nitrogen and other fluid-mobile elements (K, Rb, Cs, H) in a cold slab environment: evidence from HP to UHP oceanic metasediments of the Schistes Lustrés nappe (western Alps, Europe). Earth Planet. Sci. Lett. 215, 27–42.
Busigny, V., Cartigny, P., Philippot, P., 2011. Nitrogen isotopes in ophiolitic metagabbros: A re-evaluation of modern nitrogen fluxes in subduction zones and implication for the early Earth atmosphere. Geochim. Cosmochim. Acta 75, 7502–7521.
Cartigny, P., Palot, M., Thomassot, E., Harris, J.W., 2014. Diamond formation: a stable isotope perspective. Annu. Rev. Earth Planet. Sci. 42, 699–732.
Cibin, G., Mottana, A., Marcelli, A., Brigatti, M.F., 2005. Potassium coordination in trioctahedral micas investigated by K-edge XANES spectroscopy. Mineral. Petrol. 85, 67–87.
Cooper, D.C., Bradley, A.D., 1990. The ammonium content of granites in the English Lake District. Geol. Mag. 127, 579–586.
Downs, R.T., Andalman, A., Hudacsko, M., 1996. The coordination numbers of Na and K atoms in low albite and microcline as determined from a procrystal electron-density distribution. Am. Mineral. 81, 1344–1349.
Elkins, L.J., Fischer, T.P., Hilton, D.R., Sharp, Z.D., McKnight, S., Walker, J., 2006. Tracing nitrogen in volcanic and geothermal volatiles from the Nicaraguan volcanic front. Geochim. Cosmochim. Acta 70, 5215–5235.
Feng, L., Li, H., Liu, W., 2018. Nitrogen mass fraction and isotope determinations in geological reference materials using sealed-tube combustion coupled with continuous-flow isotope-ratio mass spectrometry. Geostand. Geoanalytical Res. 42, 539–548.
Fischer, T.P., Hitton, D.R., Zimmer, M.M., Shaw, A.M., Sharp, Z.D., Walker, J.A., 2002. Subduction and recycling of nitrogen along the Central American margin. Science 297, 1154–1157.
Förster, M.W., Foley, S.F., Alard, O., Buhre, S., 2019. Partitioning of nitrogen during melting and recycling in subduction zones and the evolution of atmospheric nitrogen. Chem. Geol. 525, 334–342.
Gardiner, C.I., Reynolds, S.H., 1932. The Loch Doon "Granite" Area, Galloway. Q. J. Geol. Soc. 88, 1.
Goldblatt, C., Claire, M.W., Lenton, T.M., Matthews, A.J., Watson, A.J., Zahnle, K.J., 2009. Nitrogen-enhanced greenhouse warming on early Earth. Nat. Geosci. 212 (2), 891–896.
Haendel, D., Muehle, K., Nitzsche, H.-M., Stiehl, G., Wand, U., 1986. Isotopic variations of the fixed nitrogen in metamorphic rocks. Geochim. Cosmochim. Acta 50, 749–758.
Halama, R., Bebout, G.E., John, T., Scambelluri, M., 2014. Nitrogen recycling in subducted mantle rocks and implications for the global nitrogen cycle. Int. J. Earth Sci. 1037 (103), 2081–2099.
Halama, R., Bebout, G.E., Bea, F., 2021. Nitrogen loss and isotopic fractionation during granulite-facies metamorphism in the lower crust (Ivrea Zone, NW Italy). Chem. Geol. 584, 120475.
Hall, A., 1987. The ammonium content of Caledonian granites. J. Geol. Soc. London. 144, 671–674.
Hall, A., 1988. The distribution of ammonium in granites from South-West England. J. Geol. Soc. London. 145, 37–41.
Hall, A., 1999. Ammonium in granites and its petrogenetic significance. Earth Sci. Rev. 45, 145–165.
Hall, A., Periera, M.D., Bea, F., 1996. The abundance of ammonium in the granites of central Spain, and the behaviour of the ammonium ion during anatexis and fractional crystallization. Mineral. Petrol. 56, 105–123.
Halliday, A.N., Aftalion, M., van Breemen, O., Jocelyn, J., 1978. Petrogenetic significance of Rb-Sr and U-Pb isotopic systems in the 400 Ma old British Isles granitoids and their hosts. Geol. Soc. Spec. Publ. 8, 653–661.
Halliday, A.N., Stephens, W.E., 1984. Crustal controls on the genesis of the 400 Ma old Caledonian granites. Phys. Earth Planet. Inter. 35, 89–104.
Halliday, A.N., Stephens, W.E., Harmon, R.S., 1980. Rb-Sr and O isotopic relationships in 3 zoned Caledonian granitic plutons, southern uplands, Scotland: Evidence or varied sources and hybridization of magmas. J. Geol. Soc. London. 137, 329–348.
Harris, B.J.R., De Hoog, J.C.M., Halama, R., 2022. The behaviour of nitrogen during subduction of oceanic crust: Insights from in situ SIMS analyses of high-pressure rocks. Geochim. Cosmochim. Acta 321, 16–34.
Higuchi, H., Nagasawa, H., 1969. Partition of trace elements between rock-forming minerals and the host volcanic rocks. Earth Planet. Sci. Lett. 7, 281–287.
Hilton, D.R., Fischer, T.P., Marty, B., 2002. Noble gases and volatile recycling at subduction zones. Rev. Mineral. Geochem. 47, 319–370.
Hines, R., Paterson, S.R., Memeti, V., Chambers, J.A., 2018. Nested incremental growth of zoned upper crustal plutons in the Southern Uplands Terrane, UK: Fractionating, mixing, and contaminated magma fingers. J. Petrol. 59, 483–516.
Honma, H., Itihara, Y., 1981. Distribution of ammonium in minerals of metamorphic and granitic rocks. Geochim. Cosmochim. Acta 45, 983–988.
Houlton, B.Z., Morford, S.L., Dahlgren, R.A., 2018. Convergent evidence for widespread rock nitrogen sources in Earth's surface environment. Science 360, 58–62.
Huang, T.-Y., Teng, F.-Z., Wang, Z.-Z., He, Y.-S., Liu, Z.-C., Wu, F.-Y., 2023. Potassium isotope fractionation during granitic magmatic differentiation: Mineral-pair perspectives. Geochem. Cosmochem. Acta. 343, 196–211.
Icenhower, J., London, D., 1996. Experimental partitioning of Rb, Cs, Sr, and Ba between alkali feldspar and peraluminous melt. Am. Mineral. 81, 719–734.
Itihara, Y., Honma, H., 1979. Ammonium in biotite from metamorphic and granitic rocks of Japan. Geochim. Cosmochim. Acta 43, 503–509.

Jackson, C.R.M., Cottrell, E., Andrews, B., 2021. Warm and oxidizing slabs limit ingassing efficiency of nitrogen to the mantle. Earth Planet. Sci. Lett. 553, 116615.
Johnson, B.W., Goldblatt, C., 2015. The nitrogen budget of Earth. Earth-Sci. Rev. 148, 150–173.
Koehler, M.C., Buick, R., Barley, M.E., 2019. Nitrogen isotope evidence for anoxic deep marine environments from the Mesoarchean Mosquito Creek Formation, Australia. Precambrian Res. 320, 281–290.
Kupriyanov, I.N., Sokol, A.G., Seryotkin, Y.V., Kruk, A.N., Tomilenko, A.A., Bul'bak, T. A., 2022. Nitrogen fractionation in mica metapelite under hot subduction conditions: Implications for nitrogen ingassing to the mantle. Chem. Geol. 628, 121476.
Labidi, J., Barry, P.H., Bekaert, D.V., Broadley, M.W., Marty, B., Giunta, T., Warr, O., Sherwood Lollar, B., Fischer, T.P., Avice, G., Caracausi, A., 2020. Hydrothermal $^{15}N^{15}N$ abundances constrain the origins of mantle nitrogen. Nature 580, 367–371.
Leggett, J.K., Mckerrow, W.S., Eales, M.H., 1979. The Southern Uplands of Scotland: A Lower Palaeozoic accretionary prism. J. Geol. Soc. London. 136, 755–770.
Li, L., Bebout, G.E., Idleman, B.D., 2007. Nitrogen concentration and $\delta^{15}N$ of altered oceanic crust obtained on ODP Legs 129 and 185: Insights into alteration-related nitrogen enrichment and the nitrogen subduction budget. Cosmochim. Cosmochem. Acta 71, 2344–2360.
Li, Y., Keppler, H., 2014. Nitrogen speciation in mantle and crustal fluids. Geochim. Cosmochim. Acta 129, 13–32.
Li, Y., Li, L., Wu, Z., 2021. First-principles calculations of equilibrium nitrogen isotope fractionations among aqueous ammonium, silicate minerals and salts. Geochim. Cosmochim. Acta 297, 220–232.
Li, K., Li, L., 2023a. Alteration enrichment of nitrogen in the gabbroic oceanic crust: Implications for global subducting nitrogen budget and subduction-zone nitrogen recycling. Geochim. Cosmochim. Acta. 351, 96–107.
Li, K., Li, L., 2023b. Nitrogen enrichment in the altered upper oceanic crust: A new perspective on constraining the global subducting nitrogen budget and implications for subduction-zone nitrogen recycling. Earth Planet. Sci. Lett. 602, 117960.
Li, Y., Wang, W., Wu, Z., Huang, S., 2019. First-principles investigation of equilibrium K isotope fractionation among K-bearing minerals. Geochim. Cosmochim. Acta 264, 30–42.
Li, L., Zheng, Y.-F., Cartigny, P., Li, J., 2014. Anomalous nitrogen isotopes in ultrahigh-pressure metamorphic rocks from the Sulu orogenic belt: Effect of abiotic nitrogen reduction during fluid–rock interaction. Earth Planet. Sci. Lett. 403, 67–78.
Mao, J., Zhang, Z., Wang, Y., Jia, Y., Robert, K., 2003. Nitrogen isotope and content record of Mesozoic orogenic gold deposits surrounding the North China craton. Sci. China Ser. D Earth Sci. 46, 231–245.
Marty, B., 2012. The origins and concentrations of water, carbon, nitrogen, and noble gases on Earth. Earth Planet. Sci. Lett. 313–314, 56–66.
Marty, B., Dauphas, N., 2003. The nitrogen record of crust–mantle interaction and mantle convection from Archean to Present. Earth Planet. Sci. Lett. 206, 397–410.
McKerrow, W.S., Leggett, J.K., Eales, M.H., 1977. Imbricate thrust model of the Southern Uplands of Scotland. Nature 267, 237–239.
Middlemost, E.A.K., 1994. Naming materials in the magma /igneous rock system. Earth Sci. Rev. 37, 215–224.
Mikhail, S., Howell, D., Hutchison, M., Verchovsky, A.B., Warburton, P., Southworth, R., Thompson, A.R., Jones, A.P., Mileage, H.J., 2014. Constraining the internal variability of carbon and nitrogen isotopes in diamonds. Chem. Geol. 366, 14–23.
Mikhail, S., Barry, P.H., Sverjensky, D.A., 2017. The relationship between mantle pH and the deep nitrogen cycle. Geochim. Cosmochim. Acta 209, 149–160.
Mikhail, S., Sverjensky, D.A., 2014. Nitrogen speciation in upper mantle fluids and the origin of Earth's nitrogen-rich atmosphere. Nat. Geosci. 7, 816–819.
Miles, A.J., Woodcock, N.H., Hawkesworth, C.J., 2016. Tectonic controls on post-subduction granite genesis and emplacement: The late Caledonian suite of Britain and Ireland. Gondwana Res. 39, 250–260.
Nagasawa, H., Schnetzler, C.C., 1971. Partitioning of rare earth, alkali and alkaline earth elements between phenocrysts and acidic igneous magma. Geochim. Cosmochim. Acta 35, 953–968.
Nash, W.P., Crecraft, H.R., 1985. Partition coefficients for trace elements in silicic magmas. Geochim. Cosmochim. Acta 49, 2309–2322.
Philpotts, J.A., Schnetzler, C.C., 1970. Phenocryst-matrix partition coefficients for K, Rb, Sr and Ba, with applications to anorthosite and basalt genesis. Geochim. Cosmochim. Acta 34, 307–322.
Robert, J.L., 1976. Titanium solubility in synthetic phlogopite solid solutions. Chem. Geol. 17, 213–227.
Rogers, J.R., Bennett, P.C., Choi, W.J., 1998. Feldspars as a source of nutrients for microorganisms. Am. Mineral. 83, 1532–1540.
Sano, Y., Nishio, Y., Fischer, T., Williams, S., Takahata, N., Fischer, T.P., Williams, S.N., 2001. Volcanic flux of nitrogen from the Earth. Chem. Geol. 171, 263–271.
Schauble, E.A., 2004. Applying stable isotope fractionation theory to new systems. Rev. Mineral. Geochem. 55, 65–111.
Sharp, Z., 1990. A laser-based microanalytical method for the in-situ determination of oxygen isotope ratios of silicates and oxides. Geochim. Cosmochim. Acta 54, 1353–1357.
Stüeken, E.E., Kipp, M.A., Koehler, M.C., Buick, R., 2016. The evolution of Earth's biogeochemical nitrogen cycle. Earth-Sci. Rev. 160, 220–239.
Stüeken, E.E., Boocock, T.J., Robinson, A., Mikhail, S., Johnson, B.W., 2021. Hydrothermal recycling of sedimentary ammonium into oceanic crust and the Archean Ocean at 3.24 Ga. Geology 49, 822–826.
Tindle, A.G., Pearce, J.A., 1981. Petrogenetic modelling of in situ fractional crystallization in the zoned Loch Doon pluton, Scotland. Contrib. Mineral. Petrol. 78, 196–207.
Urey, H.C., 1947. The thermodynamic properties of isotopic substances. J. Chem. Soc. 562–581.
Watson, E.B., Cherniak, D.J., Drexler, M., Hervig, R.L., Schaller, M.F., 2019. Nitrogen diffusion in silicate minerals, with implications for nitrogen transport and cycling in the lithosphere. Chem. Geol. 516, 42–58.
Yang, Y., Huang, W., Qi, Z., Xia, Q., 2022. Nitrogen retention in feldspar: implications for nitrogen transport in subduction zones. JGR Solid Earth 127.
Yuan, G., Cao, Y., Schulz, H.-M., Hao, F., Gluyas, J., Liu, K., Yang, T., Wang, Y., Xi, K., Li, F., 2019. A review of feldspar alteration and its geological significance in sedimentary basins: From shallow aquifers to deep hydrocarbon reservoirs. Earth-Sci. Rev. 191, 114–140.
Zerkle, A.L., Poulton, S.W., Newton, R.J., Mettam, C., Claire, M.W., Bekker, A., Junium, C.K., 2017. Onset of the aerobic nitrogen cycle during the Great Oxidation Event. Nature 542, 465–467.
Zhang, D., 1988. Nitrogen Concentrations and Isotopic Compositions of Some Terrestrial Rocks. The University of Chicago. PhD Thesis.